ICSO 2016

International Conference on Space Optics

Biarritz, France

18–21 October 2016

Edited by Bruno Cugny, Nikos Karafolas and Zoran Sodnik

Calibration OGSE for a multichannel radiometer for Mars atmosphere studies

J. J. Jiménez

F. J. Álvarez

M. Gonzalez-Guerrero

V. Apéstigue

et al.

esa icso proceedings cnes

International Conference on Space Optics — ICSO 2016, edited by Bruno Cugny, Nikos Karafolas, Zoran Sodnik, Proc. of SPIE Vol. 10562, 1056216 · © 2016 ESA and CNES
CCC code: 0277-786X/17/$18 · doi: 10.1117/12.2296142

CALIBRATION OGSE FOR A MULTICHANNEL RADIOMETER FOR MARS ATMOSPHERE STUDIES

J. J. Jiménez[1], F.J Álvarez[1], M. Gonzalez-Guerrero[1], V. Apéstigue [1], I. Martín[1], J. M Fernández[1], A. A. Fernán[1], I.Arruego[1]
[1]Instituto Nacional de Técnica Aeroespacial – INTA, Spain

I. INTRODUCTION

This work describes several OGSEs (Optical Ground Support Equipment) developed by INTA (Spanish Institute of Aerospace Technology – *Instituto Nacional de Técnica Aeroespacial*) for the calibration and characterization of their self-manufactured multichannel radiometers (Solar Irradiance Sensors - SIS) for planetary atmospheric studies in the frame of some Martian missions at which INTA is participating. The calibration OGSEs for these SIS have been improved from the first model in 2011. This work describes the currently used OGSE, as well as ideas for next improvement. We present some results of the DREAMS SIS [1] calibration and their error propagation to show the theoretical precision and accuracy that procedures to be presented can get.

INTA Payloads and Space Science Department is now involved in a number of scientific missions to Mars developing multichannel radiometers for atmosphere studies. INTA developed two SIS: MetSIS (a radiometer for the Mars MetNet Lander) and the DREAMS SIS (another one for Exomars´16 [1]). Currently, it is developing a new radiometer, the RDS (Radiation and Dust Sensor), for the next NASA/JPL rover, Mars2020 [3] and, in addition, INTA will develop another SIS for the lander of the Exomars´18 mission [4].

INTA Optoelectronic Payloads Laboratory led the optical calibration and characterization tasks of those sensors and it will be in charge of the next two ones. Due to the very specific characteristics of those instruments, *ad-hoc* OGSE and procedures for calibration and characterization were developed.

There are two kinds of OGSE: those used for calibration and those for the Optical Fast Verification (OFV). The Calibration OGSEs have three set-ups to characterize the responsivity and the angular and thermal dependencies. The OFV OGSE has been used to verify the optical SIS performance after every test.

All the instruments are based on Silicon photodiodes, interferential and density filters and masks that limit their Field of View (FoV). The FoV reduction has two objectives: to reduce the angular dependencies of the interferential filters and to provide a specific directionality to these photodiodes in order to study separately different areas of the sky.

Two main issues were overcome in order to develop these OGSEs: 1) the FoV of different optical channels does not point to the same direction; 2) channels optical response is not a cosine function and it does not have rotational symmetry. Three different measures have been used depending on the case: 1) integrating spheres, 2) two axes electronic goniometers and 3) a simple calibrated wedge to fit the instrument in a specific angle.

Different light sources were used: halogen and Xenon lamps, specific solar simulators with the AM0 spectrum and a simulator of the Mars light [5]. A reference triple-union solar cell and calibrated spectroradiometers were used to calibrate these light sources.

II. PRINCIPLE OF OPTICAL CALIBRATION

The SIS optical head (SIS-OH) consists in a truncated tetrahedron with 3 faces (East, South and West) 120º apart from each other in the azimuthal angle, φ, and with inclination or altitude angles, θ, of 60º to avoid dust deposition on the sensors active area and to get all three faces pointing to different areas of the sky. A photo of the SIS with angles φ and θ of its spherical system is shown in Fig. 1. There are two sensors (UV and NIR) with different wavelength ranges (WR) and different FoV at each lateral face of the tetrahedron. On the top of the truncated tetrahedron there is a hemispheric channel with a dome-shaped diffuser (Table 1).

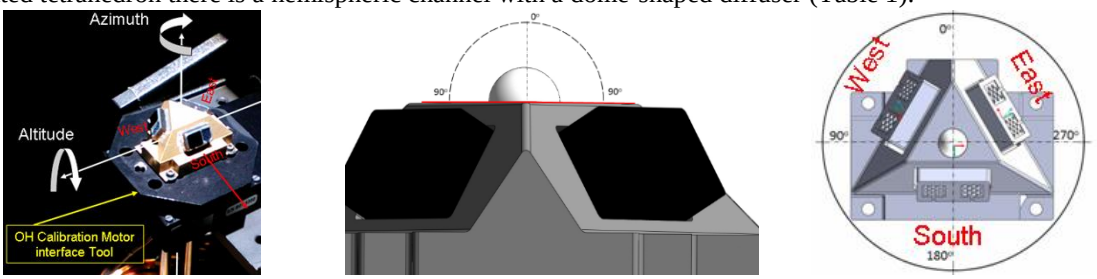

a) b) c)

Fig. 1: a) Photographic image of the DREAMS SIS for Exomars´16; b) inclination angle (θ); c) azimuthal angle (φ).

Table 1. Optical channel performance of the DREAMS SIS for the Exomars´16 mission

Face	East		South		West		Top
Orientation (φ, θ)	(300º, 60º)		(180º, 60º)		(60º, 60º)		(N.A[1], 0º) [Horizontal]
Channel	NIR_{East}	UV_{East}	NIR_{South}	UV_{South}	NIR_{West}	UV_{West}	Top
WR [nm]	700-1100	315-400	700-1100	315-400	700-1100	315-400	230-1150
FoV	±	±	±	±	±	±	±120º

[1] N.A.: Not Applicable because at θ = 0º, φ is not defined.

The method for the optical calibration of the SIS sensor is based on the spectro-radiometric transfer from a standard lamp to a standard detector in well-controlled laboratory conditions.

The output voltage of every channel of the instrument is proportional to the current (I) generated by the photodiode that is used like photodetector. This current is proportional to the incident optical power and can be expressed as a function of the irradiance (E) in the detector. The proportional factor is the responsivity (R) of the photodetector:

$$I\ (\mathrm{A}) = R\left(\mathrm{A}\cdot \mathrm{m}^2/\mathrm{W}\right)\cdot E\left(\mathrm{W}/\mathrm{m}^2\right) \tag{1}$$

Both parameters that determine the current to be given at its output by the photodetector, incident optical power and responsitivty, are functions of the wavelength (λ) and the relation is an integral. The spectral responsivity (r) also depends on the temperature (T) and on the light incident angle (α). So, (1) can be written:

$$I(T,\theta) = \int_0^\infty r(\lambda,T,\alpha)\ E(\lambda)\ d\lambda \tag{2}$$

In a first approximation, we can assume that λ, T and α are independent variables. Then, we can write:

$$r(\lambda,T,\theta) = r(\lambda)\ r(T)\ r(\alpha), \tag{3}$$

where r(α) is the Angular Response Function (ARF) and r(T) is the Thermal Response Function (TRF). Those functions are independent of the light wavelength, λ, and then:

$$I(\lambda,T,\alpha) = ARF\cdot TRF\int_0^\infty r(\lambda)\ E(\lambda)\ d\lambda \tag{4}$$

Initial conditions for TRF and ARF functions are defined to be, respectively, room temperature and a perpendicular incidence of the light on every channel's sensor. Hence, TRF is 1 at room temperature and ARF is 1 when light reaches photodiodes perpendicularly (normal incidence).

According to (4), the current (I) depends on the lamp light spectrum and on the spectral responsivity of the optical channels. The $r(\lambda)$ function depends only on the performance of the optical system (detector + optical filters) and then, it is fixed, but the mean responsivity of each channel depends on the light spectrum. For this reason, and for simplicity, a lamp with a known spectrum like the one of the Sun was used for $r(\lambda)$ calibrations. α is defined by angles (φ, θ) in the system of the unit. Then, equation (4) can be written like this:

$$I(T,\varphi,\theta,E_{Sun}) = ARF(\varphi,\theta)\cdot TRF(T)\cdot R_{Sun}\cdot E_{Sun} + offset(T) \tag{5}$$

R_{Sun} is the mean responsivity of the channel under a solar light spectrum irradiance expressed in $\mathrm{A}\cdot\mathrm{m}^2/\mathrm{W}$, E_{Sun} is the Sun irradiance expressed in W/m^2, ARF and TRF are numbers between 0 and 1 and the *offset* expressed in amperes is the sum of every offset produced by the conditioning electronics and by the dark current of the photodiode.

III. OPTICAL CALIBRATION

Three independent calibration procedures are run in order to get the three parameters of (5): the angular dependence (ARF), the thermal dependence (TRF) and the mean responsivity under sun light (R_{Sun}) of the channel calibrated:

1. **Responsivity calibration**: the optical power lamp is excited in four steps, increasing irradiance from a low level to a high one while keeping the temperature and the light angle of incidence constant over the unit. Experimental data acquired are fitted to a linear curve where the slope is the mean responsivity (R_{Sun}).
2. **Angular calibration**: optical power and temperature are fixed and only the light incidence on the sensor's surface is made to change in order to evaluate the ARF.
3. **Thermal calibration**: optical power and light angle of incidence on sensor's surface are fixed and only the temperature is made to change in order to evaluate the TRF.

The equipment used for these calibrations includes a specific SW developed in LabView as the calibration EGSE, a two axis rotator used for the control of the azimuth and inclination angles, a power supply, a specific interface between the SIS-OH and the two axis rotator (Fig. 1-a) and different light sources depending on the calibration mode (responsivity, angular or thermal).

A. Responsivity calibration

In order to set this calibration up, the AMO simulator (EP7) is switched on and its irradiance level adjusted to AM0. The light spectrum and the absolute irradiance intensity are characterized. The SIS-OH is set on the two axis rotator using the SIS-OH Motor interface tools for calibration. The top face must point upwards and the South face must be parallel to the "altitude axis" and oriented to positive spins (Fig. 1-a). The SIS is placed in the optical work plane, inside the EP7 beam, its angular orientation being levelled.

With this configuration, every face was characterized with a group of single measurements, selecting a normal incidence of the light on it. That is, light beam was pointed respectively to the South face, to the East face, to the West face and finally to the Top face. (φ, θ) coordinates are shown in Fig. 2. This was done several times in a row to get more than one point and to increase the certainty and physical meaning of the measurements and to evaluate the signal noise.

A set of measurements was done to check the possible alignment error, by sweeping the angle between the unit's face and the light beam from 0º to 60º spinning around "axis a" and "axis b" of each face (Fig. 4). The set of coordinates (φ, θ) are shown in Fig. 3.

These operations were executed under five irradiance levels. The irradiance level was controlled using a set of neutral filters. These filters are previously characterized by the SPASOLAB and they give information about the irradiance level obtained in every irradiance level and its spectral range.

At the end of the calibration, the AM0 emission was applied again on the unit in order to check any change in the signal, which might be produced by a change in the EP7 irradiance, in the SIS response (by optical degradation or heating) or in its alignment. The EP7 lamp was continuously monitored to get the adequate correction factor in case any change is detected during its emission.

The experimental data were fitted to (5) considering ARF = TRF = 1 and *offset* = 0 to get the average responsivity under Sun irradiance (R_{Sun}), see Fig. 5 and Table 2.

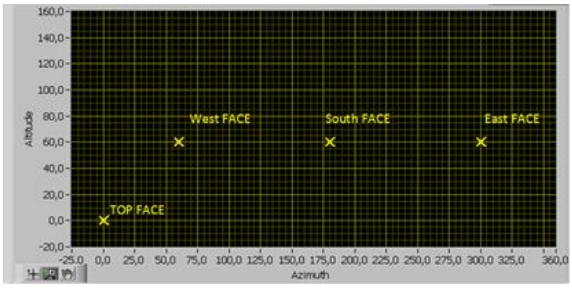

Fig. 2: Pairs of (φ, θ) coordinates selected for normal incidence on the different SIS faces

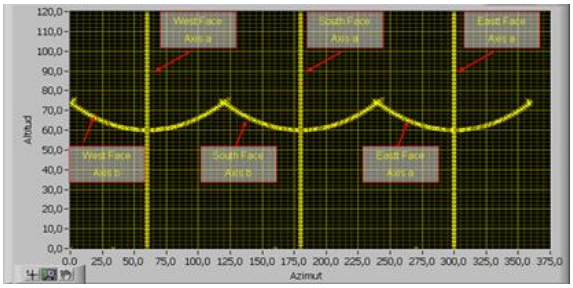

Fig. 3: Set of (φ, θ) coordinates scanned for the measurement of the alignment error

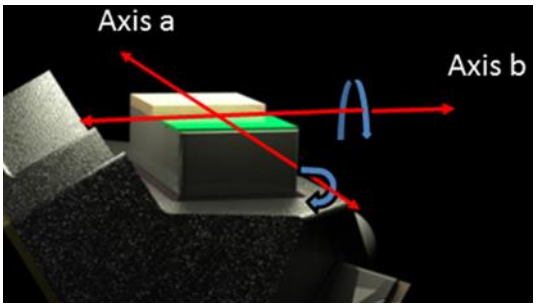

Fig. 4: Schematic drawing of the alignment error measurements

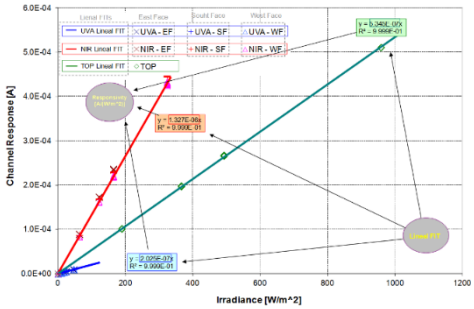

Fig. 5:SIS channels response vs. irradiance.

Table 2. Results of the responsivity calibration of the DREAMS SIS for the Exomars´16 mission

		UV_{South}	NIR_{West}	UV_{West}	NIR_{East}	UV_{East}	NIR_{South}	Top
R_{Sun}	Value	1.929E-07	2.087E-07	2.048E-07	1.429E-06	1.394E-06	1.333E-06	5.438E-07
	Std. Error	7.2E-10	8.7E-10	5.2E-10	3.3E-09	2.5E-09	3.1E-09	1.7E-09

Note: the fitting equation is **(5)** fixing ARF = TRF = 1 and *offset* = 0.

B. Thermal calibration

This procedure is used to get the TRF of the SIS optical channels, their offset, the dark current as a function of the temperature and the calibration of the temperature sensor.

In order to configure the system for this measurement, the solar simulator is switched on and its irradiance level is adjusted. The light spectrum and the absolute irradiance intensity are characterized. The monitoring sensor is set on the device and the acquisition system is started. The flight spare unit (the one that is finally flying to Mars, called SP) was placed, horizontally, on a thermal chamber with a quartz window ~40 cm of diameter. The chamber has to be closed and carefully dried. The window of the chamber is placed under the light beam of the solar simulator (EP7). The calibration EGSE is configured to perform a measurement with every channel every 30 seconds.

In this configuration, the temperature is scanned firstly from 40º to -110ºC, and back from -110º C to 40º C. Step by step, the temperature describes a ramp-up and then a ramp-down. As with the responsivity calibration, the EP7 lamp has to be continuously monitored.

The procedure has to be repeated with the chamber quartz windows covered. In this way, we get the real *offset* of all channels that is not going to be shown in this work. Every calibration takes longer than 8 hours.

In the horizontal configuration, when SIS lateral faces do not point to the light source, Top and NIR channels signal decrease to less than 10 % up to – 110º C, but UV channels show a different thermal dependence: their signal falls about ~25% (Fig. 6). Interferential filters might be showing a different thermal dependency as a function of λ and of the angle of incidence in the FoV range. In the horizontal configuration, the light incident angle is just in the limit of the FoV, especially in the UV, and the output might be quite different to the one at light normal incidence For this reason, this calibration was repeated setting the Field Campaign Model (FCM) at (φ, θ) = (180º, 60º) by the use of a calibrated wedge. In this configuration, the South face points directly to the light source. It was found that, under normal incidence, all channels have the same thermal dependency. Hence, the characterization in the horizontal configuration is dismissed for UV channels. Calibration data from this procedure are fitted to:

$$TRF(\Omega) = 1 + P_5(R_{\mathrm{PT1000}}(\Omega) - 1160) + P_6(R_{\mathrm{PT1000}}(\Omega) - 1160)^2 \qquad (6)$$

TRF UV data measured in horizontal configuration are not valid, although they are similar to the others channels (NIR and Top) that are valid. Then we take advantage of this similar and the whole number of data obtained (with NIR and Top channels) has been used to fit the UV TRF parameters. This is why the three UV channels have the same parameters and the goodness of the fitting is not good. As will be shown at the end of this work, the UV channels show a worst accuracy at low temperatures. Fig. 7 shows the experimental data and fitting lines of the NIR and Top channels, as well as the fitted UV line. Table 3 shows the P_5 and P_6 parameters of the fitting and their standard errors. The TRF accuracy is given by:

$$TRF_{accuracy}(T) = \sqrt{\left[(R(\Omega) - 1160)^2 \cdot \varepsilon_{P_6}\right]^2 + \left[(R(\Omega) - 1160) \cdot \varepsilon_{P_5}\right]^2 + \left[\left(P_5 + 2P_6 \cdot 1160R(\Omega) - 2P_6 \cdot R(\Omega)\right)\varepsilon_{R(\Omega)}\right]^2}, \qquad (7)$$

which is calculated from (6) and is shown in Fig. 8.

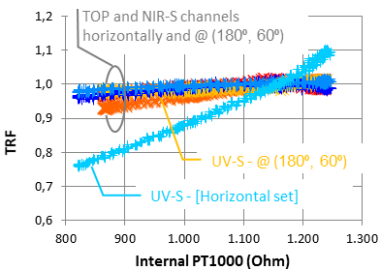

Fig. 6:TRF vs. temperature of SIS channels in horizontal and normal incidence configurations

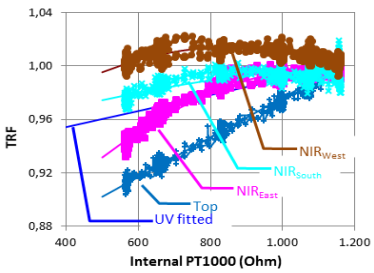

Fig. 7:TRF vs. temperature

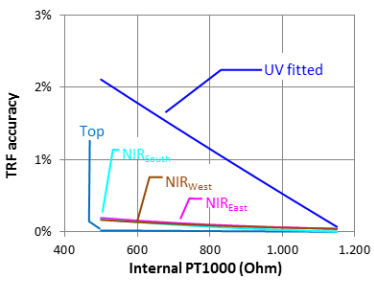

Fig. 8: TRF accuracy vs. temperature

Table 3. Responsivity calibration result of DREAMS SIS for the Exomars´16 mission

		UV	NIR_{West}	NIR_{East}	NIR_{South}	Top
P_5	Value	6.013E-05	-9,23E-05	1,2E-06	1,84E-05	1,4831E-04
	Std. Error	7.7E-07	1,2E-06	1,3E-06	1,6E-06	2,6E-07
P_6	Value	--	-1,504E-07	-1,554E-07	-3,092E-08	--
	Std. Error	--	2,3E-09	2,5E-09	3,1E-09	--

Note: (6) is used as the fitting equation .

C. Angular calibration

The light source used in this calibration is a Xenon lamp, the SIS-OH is set on the two axis rotator and the system is placed at a distance of ~4.5 meters from the Xenon lamp, where the wavefront of the Xenon light is flat enough for this calibration. The alignment is performed with a set of mirrors and its repeatability was estimated to be better than 0.5º. At (φ, θ) = (xº,0º) the top face points directly to the Xenon lamp while at (180º, 60º) it points to the South face. Sun light spectrum is not needed for this characterization because this measurement is relative. The most important condition is to keep light constant. With this aim, the lamp is switched on 45 minutes before the measurement to avoid spectral changes and its irradiance is monitored to check and compensate for the variations if existing. Both at the beginning and at the end of the of this calibration, groups of single measurements are performed with normal incidence of the light on every face (like in Fig. 2) in order to to evaluate changes in the alignment of the unit or any possible degradation.

This calibration can be divided in two processes:

a. **Perpendicular sweeping**: measurements are obtained while sweeping the angle between the unit's face and the light beam from 0º to 90º spinning around the "axis a" and the "axis b" of each face (Fig. 4). The set of 1600 pairs of (φ, θ) are shown in Fig. 9.
b. **Full matrix coverage**: measurements are obtained while sweeping θ from 0 to 120º in steps of 5º and φ from 0 to 360º in step of 5º. The set of 1728 pairs of (φ, θ) is shown in Fig. 10.

The ARF of every channel is obtained by processing this set of data, and can be represented by means of a color map in the (φ, θ) plane [7]. Seven color maps have been represented: one for the Top channel (Fig. 11) (the Top channel), three for the NIR channels, one map per channel (Fig. 13) and three for the UV channels, one map per channel (Fig. 14). The Fig. 12 shows a section of the Top surface at several azimuths (φ = 0º, φ = 60º, φ = 120º, φ = 180º, φ = 240º and φ = 300º).

The ARF accuracy is given by the equation:

$$\mathrm{ARF}_{\mathrm{accuracy}} = \sqrt{\left(\frac{\partial \mathrm{ARF}(\varphi,\theta)}{\partial \mathrm{I}}\varepsilon_{\mathrm{I}}\right)^2 + \left(\frac{\partial \mathrm{ARF}(\varphi,\theta)}{\partial \alpha_{\mathrm{sun}}}\varepsilon_{\varphi}\right)^2 + \left(\frac{\partial \mathrm{ARF}(\varphi,\theta)}{\partial \theta_{\mathrm{sun}}}\varepsilon_{\theta}\right)^2}, \quad (8)$$

where ε_I is the electrical noise of the channels signal (it has been evaluated < 0,1 %) and ε_φ and ε_θ are related to the uncertainty of the light incident angle, because the uncertainty of the Sun position might be important. Fig. 15, Fig. 16 and Fig. 17 show the accuracy of the percentage under the assumption that $\varepsilon_\varphi = \varepsilon_\theta = 1°$.

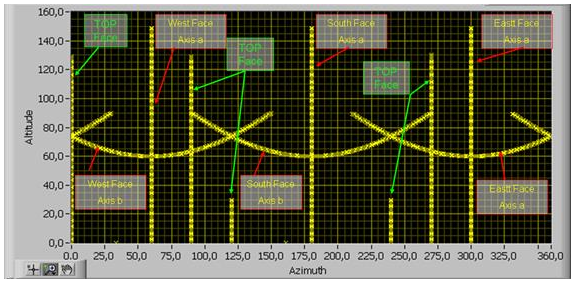

Fig. 9:Pairs of (phi, theta) coordinates in the perpedicular sweeping calibration procedure

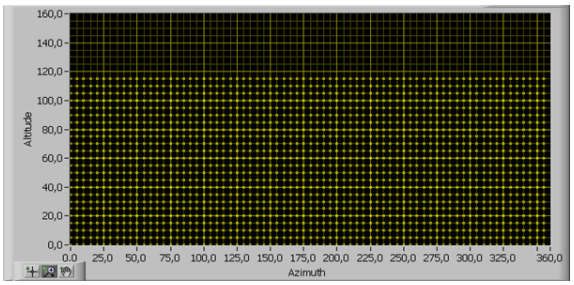

Fig. 10: Pairs of (phi, theta) coordinates in the full matrix coverage calibration procedure

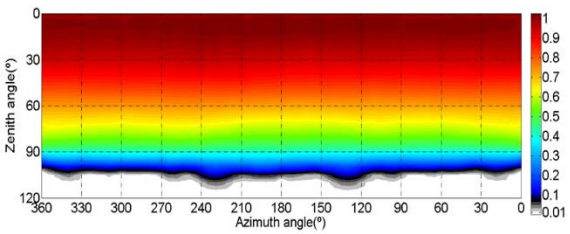

Fig. 11: Top channel responsivity colour map respect to zenith and azimuth angles

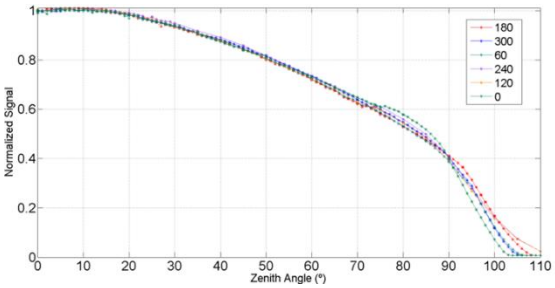

Fig. 12: Section of the top surface ARF at several azimuths

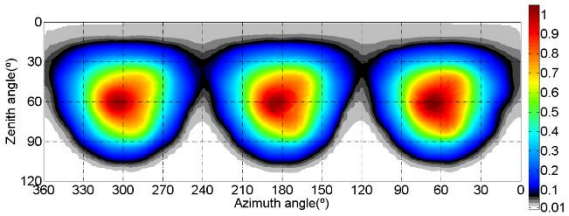

Fig. 13: Colour map of the ARF as a function of Phi and Theta for the NIR channels

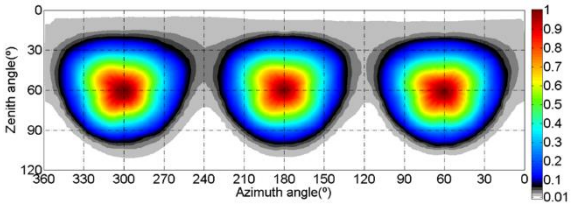

Fig. 14: Colour map of the ARF as a function of Phi and Theta for the UV channels

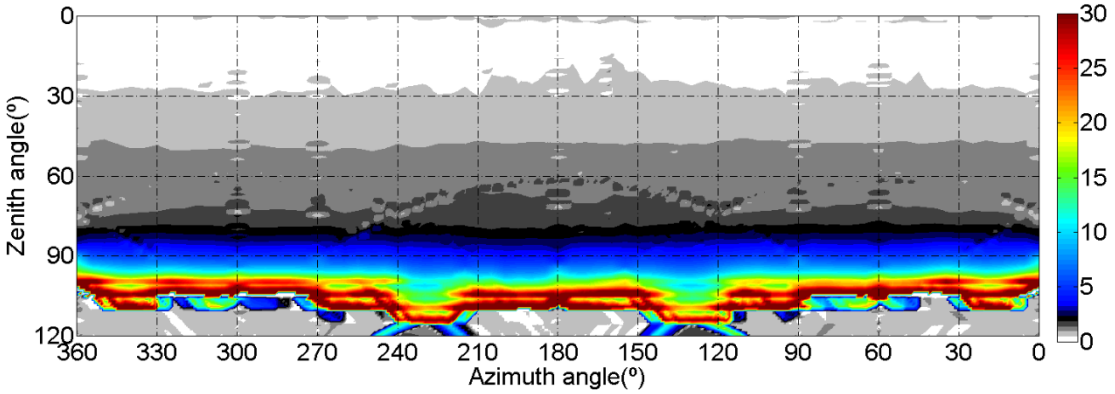

Fig. 15: Colour map of the ARF accuracy as a function of Phi and Theta for the top channel

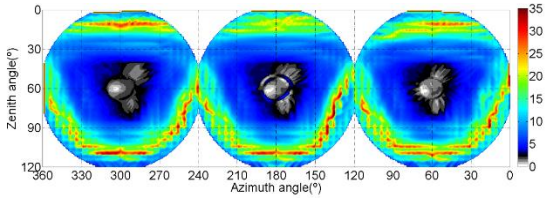

Fig. 16: Colour map of the ARF accuracy as a function of Phi and Theta for the NIR channels

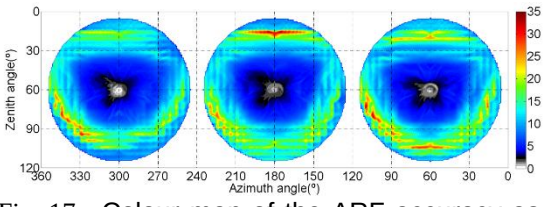

Fig. 17: Colour map of the ARF accuracy as a function of Phi and Theta for the UV channels

IV. OPTICAL FAST VERIFICATION

The Optical Fast Verification (OFV) is a quick procedure to check the basic performance of the unit along the qualification or acceptance testing performed on the developed models (FM, QM and SP), including further processes, as for example a Dry Heat Microbial Reduction (DHMR).

The goal of an OFV procedure is to get some parameters that give us reliable information about the performance of this SIS in a simple way, not requiring large facilities nor equipment (Sun simulators, temperature chambers, angular positioners…).

OFV is performed with a laptop running the calibration EGSE, a 300 mm integrating sphere (Fig. 18) with a halogen lamp, a power supply controlled by GPIB and a specific interface (Fig. 19) between the SIS Optical Head and the Integrating Sphere

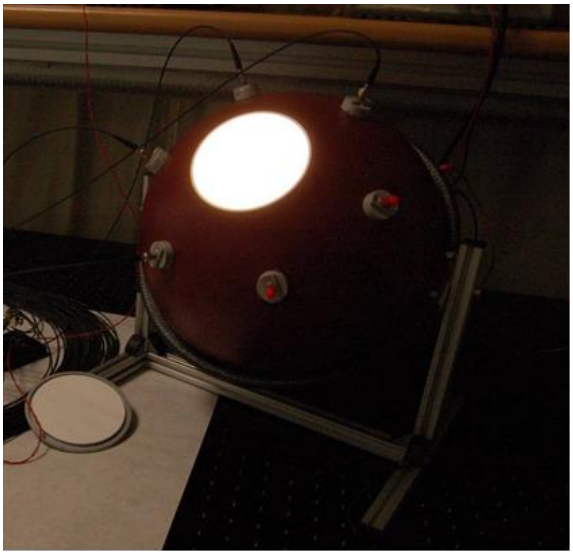

Fig. 18 the 300 mm integrating sphere for fast verification procedures

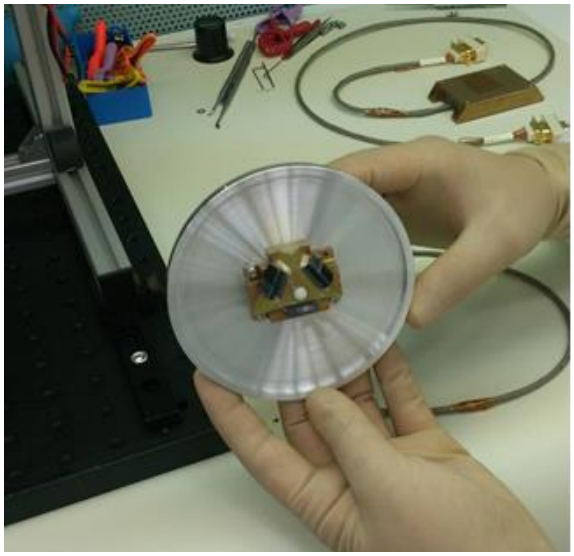

Fig. 19: Specific interface between the SIS and the power supply

The SIS-OH is set into the sphere, the light inside of the sphere is turned up step by step and some SIS parameters are measured in every step. The EGSE simultaneoulsty manages the SIS and the power supply which controls the power supply.

The EGSE stores the output of the SIS channels and its voltage references as well as the the halogen lamp bias, amongst others signals needed to check the communication protocol.

The irradiance that reaches the SIS-OH is proportional to this expression:

$$E' = V^2 \cdot I, \tag{9}$$

where E' is called pseudo-irradiance and V and I are the bias applied to the halogen lamp. There is a factor of proportionality between the irradiance and the pseudo-irradiance:

$$E = k \cdot E' \tag{10}$$

k depends on geometric issues, and for this reason, an integrating sphere and a specific interface must be used. Any change in the integrating sphere, in the alignment or even in the lamp emission, might produce a change in k. For this reason, k was evaluated with a reference optical sensor plugged in the fiber optics port. No variation in the conditions was observed along the calibration, and the pseudo-responsivity (R') was defined as

$$I = R' \cdot E' + offset, \tag{11}$$

where R' is the parameter that has been used to evaluate any possible change in the optical behavior of the SIS-OH. Fig. 20 shows the channels data, the pseudo-irradiance and the fit of one of the OFV. Fig. 21 shows a zoom of the UV channels.

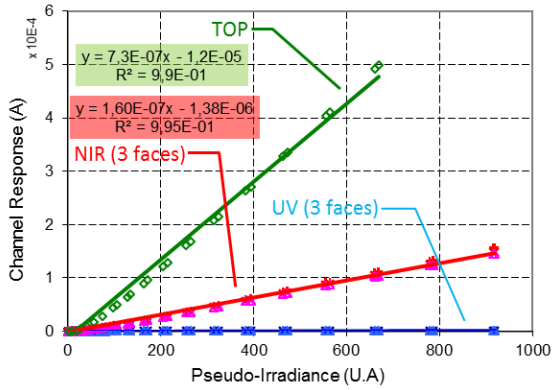

Fig. 20: SIS channels response vs. pseudo-irradiance

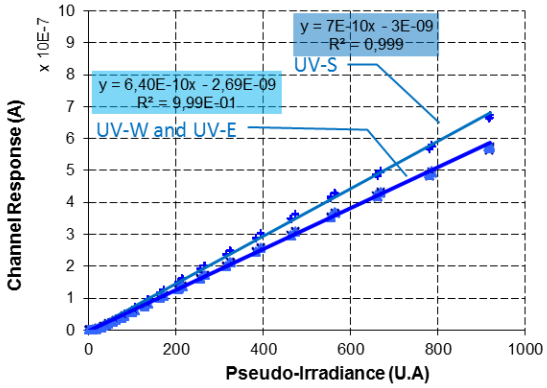

Fig. 21: Zoom of the SIS UV channels response vs. pseudo irradiance

V. CONCLUSIONS

The absolute irradiance measured by the SIS-OH can be obtained by solving equation (5). Table 4 shows the accuracy and precision of SIS channels under direct light, calculated by applying the parameters of every channel. Results from different cases allow to compare what are the most affecting parameters on the accuracy and precision of instrument's channels.

An analytical retrieval of Table 4 allows to conclude that the TOP channel has better accuracy and precision in many situations. The thermal dependencies are more important in the UV channels (though they are under control). The accuracy depends especially of the light incidence angle. The accuracy in the determination of the light incidence angle (or Sun position while in operation) is also very important. The key point in the full calibration is to perform a good ARF characterization. The ARF characterization procedure was updated several times from the first model in 2011, and the goal has been to perform the *full matrix coverage* (Fig. 10) and its analysis. In operation, it will be decisive to determine the Sun position and the SIS orientation.

SIS improvement holds UV channels with wavelength shorter than the minimum range of given by the EP7 solar simulator. Hence, it is necessary to find a new reference light source in this range.

Regarding the thermal calibration, a characterization of the FoV as a function of the temperature might be interesting. Some changes can be expected, though they might be significant only when the FoV is smaller than 0.01.

A new setup for the OFV is being prepared. It is based on a very small, portable ad-hoc integrating sphere that includes a set of LEDs and reference sensors to provide a stable, adjustable and uniform light. This tool can be used even in the final integration, in the platform, in order to get unit's performance before closing the spacecraft.

Table 4. Optical channel performance of the DREAMS SIS for the Exomars´16 mission

	Channel signal (A)	**Pt1000 (Ω)**	**Light indent angle**	**Irradiance measured [W/m2]**	**Accuracy [%]**	**Precision [W/m2]**
TOP (case 1 / case 2)	$2\cdot10^{-4}$	500 / 1200 (-120 ºC / 25.5 ºC)	0º ± 1	410.5 / 373.7	0.3 %	0.165 / 0.150
TOP case 3	$2\cdot10^{-5}$	500 (-120 ºC)	90º ± 1	102.625	10 %	0.183
NIR (case 1 / case 2)	$1.8\cdot10^{-4}$	500 / 1200 (-120 ºC / 25.5 ºC)	60º ± 1	132.0 / 128.7	1 %	0.052
NIR case 3	$5\cdot10^{-5}$	500 (-120ºC)	90º ± 1	94.3	10 %	0.0917
NIR case 6	$5\cdot10^{-5}$	500 (-120ºC)	90º ± 4	94.3	40 %	0.0917
UV (case 1 / case 2)	$3.5\cdot10^{-6}$	500 / 1200 (-120 ºC / 25.5 ºC)	60º ± 1	18.2 / 17.56	2% / 1%	0.0164 / 0.0158
NIR case 5	$3.5\cdot10^{-6}$	1100 (25.5 ºC)	60º ± 4	128.7	4 %	0.0515

REFERENCES

[1] Apestigue, et al. "2014 DREAMS-SIS: A Miniature Instrument for the Measurement of Atmospheric Optical Depth on ExoMars 2016 EDM". *International Workshop on Instrumentation for Planetary Missions*, Greenblet, Maryland (IPM-2014)

[2] I. Arruego, et all. "Development of miniaturized instrumentation for Planetary Exploration and its application to the Mars MetNet Precursor Mission", *Proceeding of the EGU2010* Vol.12

[3] http://mars.nasa.gov/mars2020/mission/rover/

[4] http://exploration.esa.int/mars/48088-mission-overview/

[5] G. Blanco, et all "INTA-SPASOLAB Facilities Upgrading for Solar Cells Characterization under the Frame of Mars Exploration Missions" *Proceedings of the 9th European Space Power Conference*: 6-10 June 2011, Saint Raphael, France, 690, ESA Communications, Noordwijk, 2011

[6] Arruego, I., Apéstigue, V., Martínez, J., Jiménez, J.J., Rivas, J., González, M.,Álvarez, J., Azcue, J., Martín, I., Canchal, R. "Solar Irradiance Sensor on the ExoMars2016 Lander". *European Planetary Science Congress* (EPSC-2015).

[7] F. J. Álvarez Ríos, et. all "Determination of the angular response function for miniaturized radiometric instruments: application to the DREAMS-SIS instrument", unpublished.

[8] I. Arruego et. All, "DREAMS-SIS, the solar Irradiance Sensor on-board the ExoMars 2016 Lander: concept, design and operating principles", Advances in Sapce Research, unpublished.

[9] D. Toledo et. All, "Measurement of dust optical depth using the Solar Irradiance Sensor (SIS) onboard the ExoMars 2016 EDM", unpublished